

J. J. Reece · S. A. T. Redfern · M. D. Welch
C. M. B. Henderson · C. A. McCammon

Temperature-dependent Fe^{2+} – Mn^{2+} order–disorder behaviour in amphiboles

Received: 29 December 2000 / Accepted: 31 June 2002

Abstract The partitioning of Fe and Mn between the large M(4) site and the octahedral sites, M(1,2,3) in the amphibole structure has been investigated in two natural manganogrunerites of compositions $\text{Ca}_{0.1}\text{Mn}_{1.9}\text{Mg}_{1.25}\text{Fe}^{2+}_{3.56}\text{Fe}^{3+}_{0.38}\text{Si}_{7.81}\text{O}_{22}(\text{OH})_2$ and $\text{Ca}_{0.24}\text{Mn}_{1.57}\text{Mg}_{2.27}\text{Fe}^{2+}_{2.76}\text{Fe}^{3+}_{0.32}\text{Si}_{7.84}\text{O}_{22}(\text{OH})_2$. The long-range cation distribution in the two samples has been elucidated by in situ neutron powder diffraction revealing that Mn is preferentially ordered onto $\text{M}(4) \gg \text{M}(2) > \text{M}(1) > \text{M}(3)$ in both samples. Partitioning of Mn from M(4) into the octahedral sites begins at 350 °C, with site exchange energies of $-16.6 \text{ kJ mol}^{-1}$ and $-14.9 \text{ kJ mol}^{-1}$, in samples containing 1.90 and 1.57 Mn apfu, respectively. Mössbauer and infrared spectroscopy have been used to study the samples at room temperature, and Mössbauer data agree well with the diffraction results, confirming that high-temperature cation distributions are retained during cooling. The fine structure in the hydroxyl-stretching region of the IR absorption spectra has been used to discuss qualitatively the site occupancies of the coordinating M(1)M(3)M(1) triplet, linked by O(3). On the basis of such modelling, we conclude that a degree of local clustering is present in both samples.

Keywords Cation partitioning · Order–disorder · Neutron diffraction · FTIR and Mössbauer spectroscopy

Introduction

Amphiboles incorporate an extremely wide range of chemical compositions and occur across a diverse range of geological parageneses. As well as information regarding the energetically favourable equilibrium cation distributions in minerals, there is a need to understand the temperature dependence of ordering processes. In particular, cation order–disorder within the amphibole structure provides a potential indicator of thermal history. The potential of cummingtonite as a geothermometer was pointed out by Ghose and Weidner (1972), yet strenuous efforts to characterize the crystal chemistry of natural amphiboles have, seldom, been driven by such considerations. One reason for this is that the complexity of their chemistry and structure poses huge problems for thermometric calculations (Evans and Ghiorso 1995). A variety of techniques have been combined in the past to elucidate amphibole crystal chemistry but such methods can employ certain assumptions. Furthermore, the influence of short-range order within the structure is still relatively poorly understood.

Spectroscopic methods are well-proven tools, which may usefully be employed to provide insights into intracrystalline partitioning in amphibole on a shorter-length scale than that probed by average structure methods such as diffraction. The present work reports the order–disorder behaviour of two Mn-rich amphiboles as a function of temperature, measured directly by in situ powder neutron diffraction. Room-temperature infrared and Mössbauer measurements of the same samples are also reported and the cohesion of these results with that expected from consideration of the neutron-refined cation distributions is discussed.

Supplementary material The tables 2, 3 and 4 has been deposited in electronic form and can be obtained from <http://link.springer.de/link/service/journals/00269>

J. J. Reece · S. A. T. Redfern (✉) · M. D. Welch
Department of Earth Sciences, University of Cambridge,
Downing Street, Cambridge, CB2 3EQ, UK,
E-mail: satr@cam.ac.uk

M. D. Welch
Department of Mineralogy, The Natural History Museum,
Cromwell Road, London, SW7 5BD, UK

C. M. B. Henderson
Department of Earth Sciences, The University of Manchester,
Oxford Road, Manchester, M13 9PL, UK

C. A. McCammon
Bayerisches Geoinstitut, Universität Bayreuth, 95440,
Bayreuth, Germany

Samples

We have studied two manganogrunerites (formerly classified as dannemorites; Leake et al. 1997) from the collection of the Natural History Museum, London. The samples originate from near the village of Långban, an area of intensely mineralized Fe–Mn deposits in the Swedish Bergslagen Orefield. Their accession numbers are BM40798 and BM1980/280. Both samples comprised prismatic crystals bound together in a massive bulk that proved to be phase-pure after magnetic separation of crushed grains and optical inspection. Electron microprobe analyses were performed using a Cameca SX50 and sample compositions calculated by averaging 20 analyses of each specimen. Analyses of grains from different sections of the bulk sample showed no compositional variation within experimental error. The sample compositions are $\text{Ca}_{0.1}\text{Mn}_{1.9}\text{Mg}_{1.25}\text{Fe}^{2+}_{3.56}\text{Fe}^{3+}_{0.38}\text{Si}_{7.81}\text{O}_{22}(\text{OH})_2$ (BM40798) and $\text{Ca}_{0.24}\text{Mn}_{1.57}\text{Mg}_{2.27}\text{Fe}^{2+}_{2.76}\text{Fe}^{3+}_{0.32}\text{Si}_{7.84}\text{O}_{22}(\text{OH})_2$ (BM1980/280). The formulae of the two samples were taken from an average of 20 analyses, calculated on the basis of 23 oxygens and normalized on the basis of 15 cations, to take into consideration the effect of Fe^{3+} on the formula unit (Droop 1987).

Experimental

Neutron powder diffraction

Neutron powder diffraction was carried out at the POLARIS diffractometer of the ISIS neutron spallation source, Rutherford Appleton Laboratory, UK (Hull et al. 1992). The details of the instrumental parameters and experimental arrangement are given in Table 1. Approximately 5 g of each sample were loosely packed into a vanadium canister and heated under vacuum in a vanadium cylindrical furnace. Data were collected in three banks of detectors: forward scattering; 90° ; and back-scattering geometries. The latter two banks were used for structure refinement. Temperature was

measured by a thermocouple placed in direct contact with the sample can. The temperature increments used are reported in Tables 2, 3 and 4 (available as Electronic Supplementary Material). A total accumulated beam current of $300 \mu\text{A}$ was collected for each temperature (taking approximately 2 h), and determined to be sufficient to ensure satisfactory intensity statistics at a scattering vector of around 60 \AA^{-1} . At certain elevated temperatures, two datasets were collected from BM40798 in order to check for any time-dependent effect in the sample, and to see if the cation distributions observed represent merely an average (i.e. a non-equilibrium state). Data were also collected during cooling for sample BM1980/280.

All data sets were refined by Rietveld analysis (Rietveld 1969) using the GSAS program (Larson and Von Dreele 1994). Both structures were refined in space group $C2/m$ at all temperatures using data from an Mg–Mn cummingtonite structure as a starting point. The Mn was initially all entered into M(4) and the Mg and Fe was disordered over the octahedral sites before refinement. Strict compositional constraints were applied during the least-squares refinement. The number of unknown coefficients in the refinement was minimized with respect to the number of constraining equations by refining only two cations over two positional sites in any cycle. During initial refinements, the temperature factors of the cation sites displayed significant scatter during heating. As a method of minimizing such effects on site occupancies, the individual site temperature factors were constrained to a line of best fit through the scattered values. The refinements were then run, allowing cation occupancies to change. Next, the occupancies were fixed and the thermal parameters were allowed to refine. This procedure resulted in a linear increases in Uiso (Tables 3 and 4 – available as Electronic Supplementary Material). Correlations between refinable parameters were checked, and not found to be statistically significant. As an indication of the quality of the least-squares refinement, we report values of the function R_{wpb} . This is the residual calculated for the Bragg contribution to the pattern only (not including the background contribution, which can lead to a flattering assessment of the model) and is defined as:

$$R_{\text{wpb}} = \sqrt{\frac{\sum_i w_i ((I_i - I_{\text{calc}})(I_i - I_{\text{back}})/I_i)^2}{\sum_i w_i (I_i - I_{\text{back}})^2}},$$

where I_i and $I_{i,\text{calc}}$ are the observed and calculated intensities at the i th point in the pattern respectively and $I_{i,\text{back}}$ is the background contribution to the profile. The weighting, w_i is related to the estimated standard deviation in the intensity of the i th point by $w_i = 1/\sigma_i^2$.

Table 1 Experimental and instrumental parameters pertaining to the neutron data and Rietveld refinements

Instrumental	POLARIS (neutron time-of-flight powder diffractometer)
Diffractometer	12.7837 m
Flight path	58 ^3He gas tubes at 145° ; 216 ZnS scintillators at 90° 2θ
Detectors	1998–19 000 μs for 145° 2θ ; 3015–20 000 μs for 90° 2θ
Data range	$dt/t = 5 \times 10^{-3}$ at 145° 2θ , 7×10^{-3} at 90° 2θ
Time channel binning	
Refinement	
Space group	$C2/m$
Z	2
Unit-cell refinement	Whole pattern
Observations	8185
Refined parameters	
Structural	61
Profile	8 + 8 (8 for each histogram)
Background	10 + 10 coefficients of a shifted Chebyshev function
Cell	4
Constraints	
Strict (Σ site = 1)	Si + Fe (T1); Mn + Fe + Mg (M1,2,3,4); Fe M(1+2 + 3+4); Mn M(1+2 + 3+4) Mg M(1+2 + 3+4)
Thermal parameters	All atoms isotropic

Table 2 Cell parameters and fractional site occupancies of both samples as a function of temperature, refined by Rietveld analysis of neutron diffraction data. *Figures in parentheses* represent calculated error in the last digits of the result given. Note: $X_{\text{Mg}}^{\text{M}(4)} = 0$ in both samples at all temperatures (This table is available as electronic supplementary material)

Table 3 Refined atomic coordinates of sample BM40798 as a function of temperature. *Figures in parentheses* represent estimated standard deviation. Special atomic positions that are constrained by symmetry are not given (This table is available as electronic supplementary material)

Table 4 Refined atomic coordinates of sample BM1980/280 as a function of temperature. *Figures in parentheses* represent estimated standard deviation (This table is available as electronic supplementary material)

Infrared absorption spectroscopy

Infrared powder absorption spectra of the two samples were recorded at room temperature in the region $300\text{--}4500\text{ cm}^{-1}$ using a Bruker 66 V IFS spectrometer. The samples were prepared as pressed discs, diluted to 0.33 wt% of the KBr disc. The region around the hydroxyl-stretching region in these amphiboles ($3600\text{--}3700\text{ cm}^{-1}$) shows a high background, most probably due to the presence of non-structural water. This background could not be eradicated from the spectra even after holding the samples at $120\text{ }^{\circ}\text{C}$ for 90 days, and was eliminated from the spectra by fitting a background function. The fine structure in the hydroxyl region was fitted with mixed Gaussian and Lorentzian curves and the areas of these were used in attempted qualitative site occupancy calculations.

Mössbauer spectroscopy

The samples were gently ground individually in an agate mortar with acetone to make powders. These were mixed with benzophenone to avoid preferred orientation and loaded into Plexiglas sample holders, 12 mm in diameter. Sample weights were determined based on the iron composition such that the dimensionless effective sample thickness for all samples was equal to 2 (corresponding to 5 mg Fe cm^{-2}) in order to minimize thickness effects. Spectra were collected at room temperature (293 K) on a conventional transmission Mössbauer spectrometer. A spectrum was also collected from a separate specimen of sample BM1980/280 that had previously been studied at ISIS and heated to $650\text{ }^{\circ}\text{C}$ before relatively rapid cooling.

The fitting model was chosen based on both minimizing the number of parameters and providing a physically realistic fit to the spectra. The fitting model consisted of three doublets, assigned to Fe^{2+} in the $\text{M}(1)+\text{M}(2)+\text{M}(3)$ sites, Fe^{2+} in the $\text{M}(4)$ site and Fe^{3+} . Doublet line shapes were best fit with a Voigt profile, where both Lorentzian linewidth and Gaussian standard deviation were allowed to vary. Conventional assumptions were made for the high- and low-velocity components of each doublet (i.e. equal area, equal width, equal Gaussian standard deviation). No interspectrum constraints were applied.

Results

Powder diffraction

Neutron powder diffraction data were refined until convergence between model and fit was achieved. For R_{wpb} factors, see Tables 3 and 4 (available as Electronic

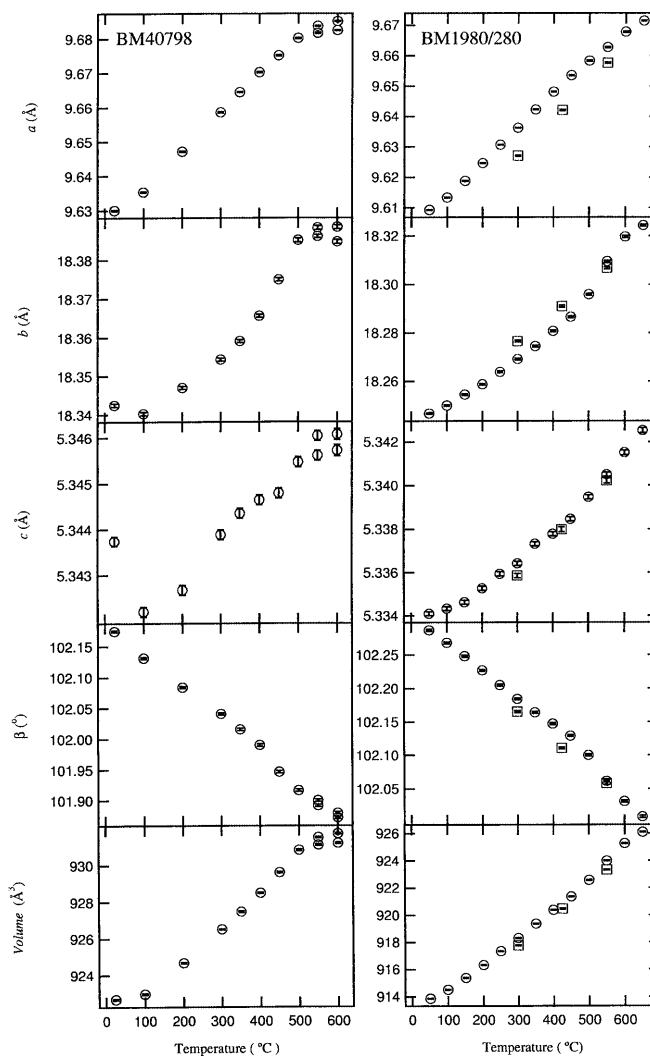


Fig. 1 Variation in cell parameters of samples BM40798 and BM1980/280 as a function of temperature

Supplementary Material). Various models of M-site exchange were used in different constraint schemes for the refinement, but the lowest residual between fit and model was found using models that employed an overall compositional constraint but no other. Cell parameters and fractional site occupancies are displayed in Table 2 (available as Electronic Supplementary Material) against temperature. Atomic coordinates and site temperature factors for samples BM40798 and BM1980/280 are displayed in Tables 3 and 4, respectively. Figure 1 displays the cell parameters of the two amphiboles over the experimental temperature range. Sample BM40798 exhibits larger values for the b and, more obviously, c cell parameters at room temperature than expected from the extrapolation of the high-temperature parameters to room temperature and we can currently offer no explanation for this. The b and c cell parameters in BM40798 are significantly larger than those of BM1980/280, reflecting the greater aggregate cation radii in BM40798.

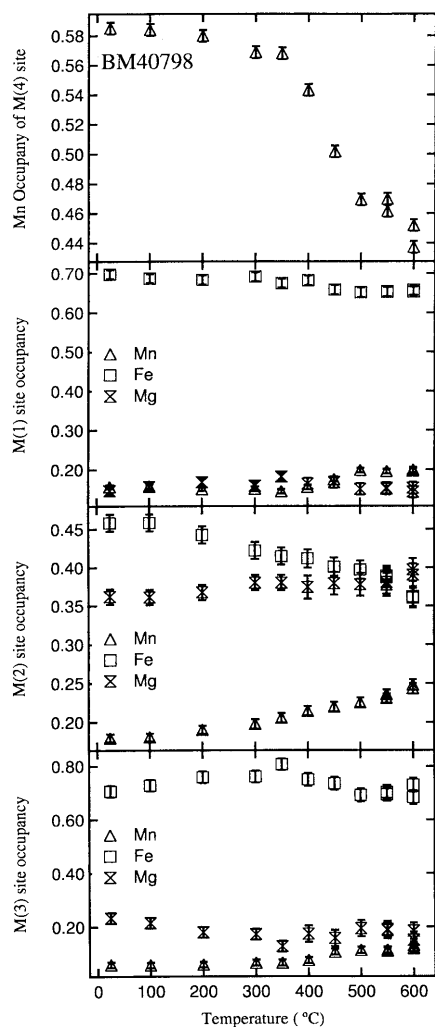


Fig. 2 Site occupancies in BM40798, as a function of temperature

The unit-cell parameters show an increase due to thermal expansion, with an inflection at 350–400 °C (most clearly observed in *b*). These changes in slope are very subtle but would be expected and interpreted as the onset of cation partitioning, in view of the results for site occupancies given below. At high temperatures, where two isothermal datasets were collected consecutively for BM40798, the cell parameters change systematically with time. The second sets display smaller cell parameters, which then increase with thermal expansion at the next temperature, before decreasing again with time when held at that temperature. In the lower-Mn sample, BM1980/280, any inflection that might represent the onset of cation partitioning between M(4) and the octahedral sites is not so clearly evident from the cell parameters. After heating and cooling, the cell parameters (in particular *a*, *b* and β) show an irreversible change.

Average site occupancies for samples BM40798 and BM1980/280 derived directly by refinement of the neutron diffraction data are displayed in Figs. 2 and 3, respectively. In both samples Mn is found to be preferentially ordered onto M(4), as expected. Partitioning

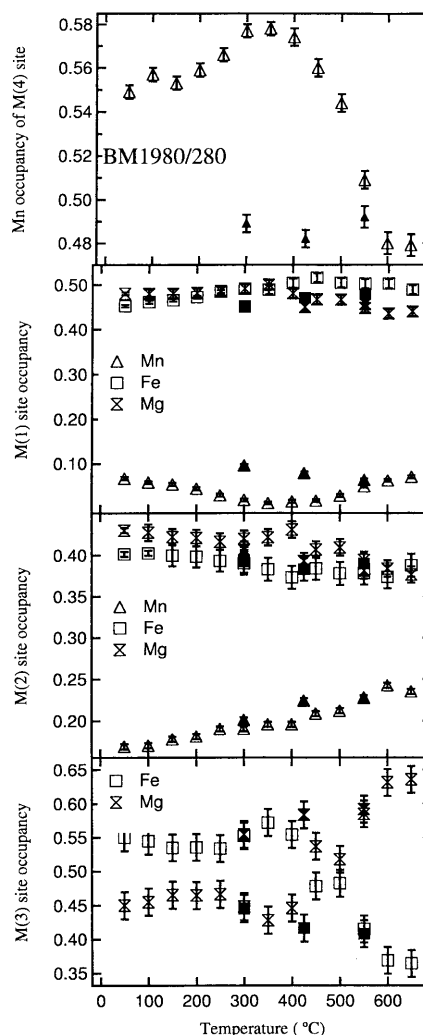


Fig. 3 Site occupancies in BM1980/280, as a function of temperature

of Mn into the octahedral sites occurs at around 350 °C. A more ordered distribution is first approached before partitioning in BM1980/280. This kind of behaviour has been noted in amphibole before (Reece et al. 2000) and is interpreted as a kinetic relaxation toward equilibrium. Within the octahedral sites, this sample, BM1980/280, shows almost no site preference between Fe and Mg but Mn shows a slight preference between $X_{\text{Mn}}^{\text{M}(2)} > X_{\text{Mn}}^{\text{M}(1)}$. The M(3) site becomes increasingly Mg-rich and this state is maintained on cooling. The octahedral sites in the Fe-rich sample, BM40798, display a strong degree of ordering of Fe and Mg. The M(1) and M(3) sites display high ratios of Fe:Mg with M(2) showing a more even distribution, especially after partitioning, as Fe leaves M(2) and enters the M(4) site in exchange for Mn. The Mn-rich sample (BM40798) contains Mn on all three octahedral sites.

Further confirmation of partitioning is available from consideration of the crystal geometry as the mean bond length for each site reflects the changing cation site occupancies. Figure 4 shows the mean bond lengths of the two samples as a function of temperature. The scales of

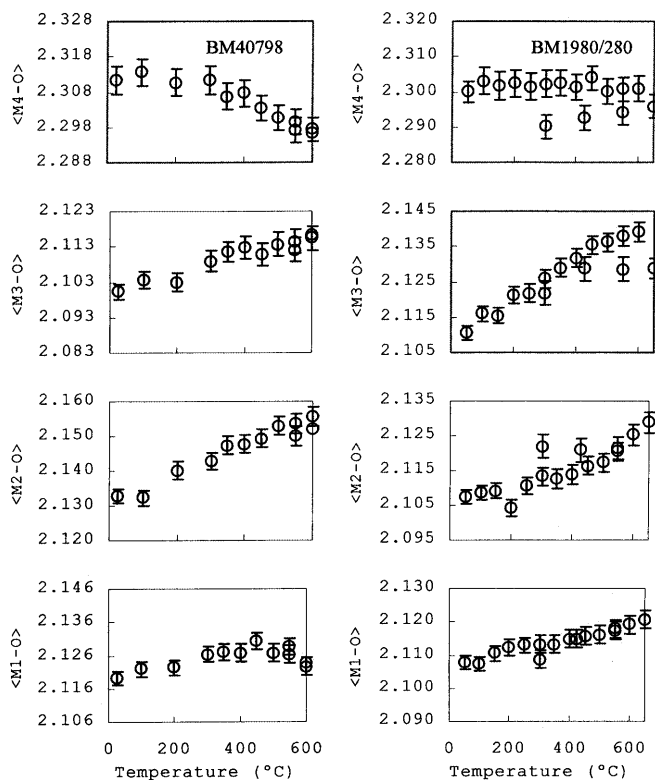


Fig. 4 The mean M(4) and octahedral site cation–oxygen bond lengths of both samples during heating

the individual graphs are the same for meaningful comparison of changes in the bond lengths during heating. The most marked changes, other than simply thermal expansion, are in $\langle M4-O \rangle$, $\langle M2-O \rangle$ and $\langle M3-O \rangle$. Considering the magnitude of the changes in mean bond lengths and the associated standard deviation in the precision of these figures, one must be cautious when applying a linear or bilinear fit to the data. Increases and decreases in mean octahedral bond lengths are consistent with changes in site occupancies. In the case of BM1980/280, the mean bond length $\langle M4-O \rangle$ shows less significant change during disorder. This might reflect the fact that this sample contains over twice as much Ca^{2+} at M(4) and hence the effect of Fe–Mn exchange is diluted somewhat.

Mössbauer spectroscopy

The spectra of both samples (Fig. 5) are similar to those reported for amphibole in the literature, and consist of overlapping components due to Fe^{2+} occupying the octahedral sites [one or more of M(1), M(2), M(3) and M(4)] and Fe^{3+} . The Fe^{2+} M(4) and Fe^{3+} contributions are well resolved in each of the spectra, so it is possible to determine robust values for the relative site distributions. The relative areas of the different components and site iron contents are given in Table 5. The Mössbauer site occupancies agree very well, within error, with those of neutron diffraction refinements, although there are dif-

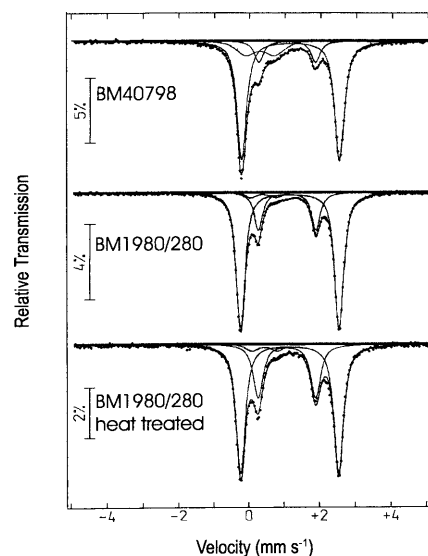


Fig. 5 Mössbauer spectra of the two samples showing quadrupole doublets of ^{57}Fe , resolved into contributions from Fe^{2+} at M(1,2,3) = outer doublet, Fe^{2+} at M(4) = inner doublet and Fe^{3+} = broad doublet with low intensity. Note that two separate samples of BM1980/280 were analyzed, one of which had been to high temperature at ISIS

ferences with regard to the inferred Fe^{3+} content of each sample. There is more than one set of hyperfine parameters for Fe^{3+} absorption due to distribution over the several crystallographic sites, but resolution restricts fitting to just one doublet. The Mössbauer results confirm that the degree of disorder on the M(4) site in the sample heat-treated at ISIS is retained to room temperature. This result confirms the trends observed in Fig. 3 and also observed in Mn–Mg cummingtonite (Reece et al. 2000).

Infrared absorption spectroscopy

The relationship between cation occupancies of the coordinating M(1) and M(3) triplet around the O(3)–H vector and the relative intensities of the fine structure of the OH infrared absorption band has been the subject of much debate since the correlation was first suggested by Burns and Strens (1966). The equations relating M(1)M(3)M(1) configuration to the relative band intensities in binary amphiboles as used by Law (1976) are shown below. In our case, the contributions to the fine structure of Mn^{2+} and Fe^{2+} are considered to overlap and are therefore called (M^{2+}). The relative shifts of the intermediate absorbance bands of the hydroxyl stretching regions in our samples are consistent with those reported for Mg–Fe binary amphiboles by Strens (1974). Our neutron data reveal significant long-range ordering (LRO) over the three sites, as well as between them and M(2) and M(4). Any non-random cation distribution will modify the conditional probabilities of occurrences of triplets of metal cations around the hydroxyl. For a binary composition $C2/m$ amphibole the fractional peak

Table 5 Resolved peak areas of the contributing elements to the ^{57}Fe quadrupole doublets and calculated Fe occupancies of the M(4) and M(1,2,3) sites. *Figures in parentheses* represent errors in the last digits of given results

Sample	Total Fe ^a a.p.f.u.	Fe ²⁺ M(1+2+3) (%)	Fe ²⁺ M(4) (%)	Fe ³⁺ (%)	Fe ²⁺ M(1+2+3) a.p.f.u.	Fe ²⁺ M(4) a.p.f.u.	Fe ³⁺ a.p.f.u.
BM40798 Rietveld	3.94	–	–	–	2.88 (0.004)	0.68 (0.004)	0.38 (0.004) ^b
BM40798 Mössbauer	3.94	72 (3)	12 (3)	16 (2)	2.84 (0.12)	0.47 (0.12)	0.63 (0.16)
BM1980/280 Rietveld	3.08	–	–	–	2.15 (0.013)	0.61 (0.013)	0.32 (0.013) ^b
BM1980/280 Mössbauer	3.08	75 (3)	21 (3)	4 (2)	2.31 (0.09)	0.65 (0.09)	0.12 (0.06)
BM1980/280 heat-treated	3.08	66 (3)	29 (3)	5 (2)	2.03 (0.09)	0.89 (0.09)	0.15 (0.06)

^a Average of 20 electron microprobe analyses^b See discussion on calculation of trivalent iron

areas are then related to the site occupancies according to the relations:

$$\text{MgMgMg} = [\text{Mg}]^{\text{M}(1)}[\text{Mg}]^{\text{M}(3)}[\text{Mg}]^{\text{M}(1)}$$

$$\text{MgMg}(\text{M}^{2+}) = 2\{[\text{Mg}]^{\text{M}(1)}[\text{Mg}]^{\text{M}(3)}[\text{M}^{2+}]^{\text{M}(1)}\} \\ + [\text{Mg}]^{\text{M}(1)}[\text{M}^{2+}]^{\text{M}(3)}[\text{Mg}]^{\text{M}(1)}$$

$$\text{Mg}(\text{M}^{2+})(\text{M}^{2+}) = 2\{[\text{Mg}]^{\text{M}(1)}[\text{M}^{2+}]^{\text{M}(3)}[\text{M}^{2+}]^{\text{M}(1)}\} \\ + [\text{M}^{2+}]^{\text{M}(1)}[\text{Mg}]^{\text{M}(3)}[\text{M}^{2+}]^{\text{M}(1)}$$

$$\text{and } (\text{M}^{2+})(\text{M}^{2+})(\text{M}^{2+}) = [\text{M}^{2+}]^{\text{M}(1)}[\text{M}^{2+}]^{\text{M}(3)}[\text{M}^{2+}]^{\text{M}(1)}.$$

If $[\text{Mg}]^{\text{M}(1)} = x$; and $[\text{Mg}]^{\text{M}(3)} = y$; then the triplet peak area fractions can be expressed as;

$$\text{MgMgMg} = x^2y \quad (1)$$

$$\text{MgMg}(\text{M}^{2+}) = x^2 + 2xy + 3x^2y \quad (2)$$

$$\text{Mg}(\text{M}^{2+})(\text{M}^{2+}) = 2x + y - 4xy + 3x^2y - 2x^2 \quad (3)$$

$$(\text{M}^{2+})(\text{M}^{2+})(\text{M}^{2+}) = (1-x)^2(1-y) \quad (4)$$

Given the relative peak areas, it is possible to solve Eqs. (1) to (4) simultaneously, by minimizing the value of $R = \sum_i (I_i^C - I_i^O)^2$, where I_i^C and I_i^O represent calculated and observed relative intensities at the i th band. This gives a best-fit solution for x and y and hence, the distribution of Mg over the C-group sites (note, $X_{\text{Mg}}^{\text{M}(2)}$ is calculated by difference from $X_{\text{Mg}}^{\text{Total}}$, since $X_{\text{Mg}}^{\text{M}(4)} = 0$, from diffraction). We note, however, that this model neglects possible effects of short-range interactions at the M(1), M(3) and M(1) sites. It assumes that the short-range order (SRO) is equal to the long-range order and, in effect, gives an account of the long-range structure as an average of clusters. By LRO we mean cation order that exists over a long correlation length (many tens of unit cells) in the crystal, as is typically given by a diffraction experiment from the average occupancies of each site. In contrast, SRO is a measure of cation self-avoidance on a nearest-neighbour and next-nearest-neighbour length scale. Comparison of the infrared data with the average site occupancies given by Rietveld refinements provides a route to explore the deviation between the short-range and long-range order. We note that the discussion of SRO and its definition in amphi-

boles (Whittaker 1979; Hawthorne et al. 1996), and other minerals has been made in the literature and we make no further contribution here, other than to treat the results generated by the above equations in a qualitative manner. Furthermore, we acknowledge that the treatment of the relative intensities of the stretching mode of the O–H in such a way ignores the effect of cation configuration on the coupling term between the electromagnetic field and the O–H dipole. The data of Skogby and Rossman (1991) were used to calculate linearly adjusted, normalized, relative peak areas, and these were also used in solving x and y . Della Ventura et al. (1996) questioned the model of Skogby and Rossman (1991) when examining synthetic (Mg, Ni)- and (Mg, Co)-potassium-richrichterite and comparing relative band intensities as a function of long-range triplet composition based upon previous Rietveld refinements. Hence, the situation is still confused and we report observed peak areas as well as values, taking into account a correction using the data of Skogby and Rossman.

Two infrared absorption spectra in the region 3580–3700 cm^{-1} , obtained from the samples at room temperature, are shown in Fig. 6. Both spectra contain four peaks corresponding to configurations on M(1) and M(3) that are annotated on the spectra. Note that the peak due to a Mg–Mg–Mg configuration is very weak in sample BM40798. The relative areas of the mixed Gaussian/Lorentzian peaks used to fit the experimental data are shown in Table 6. Neither of the spectra indicates the presence of trivalent iron at either the M(1) or M(3) sites. This would generate asymmetry in the peak shapes to the low-frequency side of the main band positions that is not seen in our spectra. Frequency-corrected areas are presented with the original observed areas in Table 6, with corresponding values of R for each least-squares fit. When applied to our spectra, the Skogby and Rossman correction made no improvement to the differences between the site occupancies derived from the raw infrared spectra and Rietveld refinement.

Considering the results of Table 6 qualitatively, and assuming that our diffraction results provide an accurate measure of the LRO, then in the case of BM40798, the infrared spectrum shows a degree of SRO that differs from the LRO: the infrared peak areas suggest higher proportions of $\text{M}^{2+}\text{M}^{2+}\text{Mg}$ and MgMgM^{2+} clusters

relative to the other configurations. In contrast, the infrared results for BM1980/280 imply a greater number of end-member triplets ($M^{2+} M^{2+} M^{2+}$ and $MgMgMg$) relative to the other possible configurations, as calculated from diffraction data. The differences are not large, but taken at face value these results seem to imply that there is a tendency towards $Fe^{2+}-Fe^{2+}$ avoidance in the Fe-rich sample BM40798 but Fe and Mg clustering in BM1980/280. This apparent contradiction, if real, is

presumably a consequence of the different compositions of the two samples. This difference is primarily in the Fe:Mg ratio, being 3.0 in the former sample and 1.3 in the latter. It is feasible that the degree of SRO varies with composition, since it has been generally observed that SRO will tend to show greater differences from LRO in more dilute systems (Myers et al. 1998). In addition, we note that BM40798 contains more Fe^{3+} (according to Mössbauer measurements) than BM1980/280, and that this extra Fe^{3+} is likely to occupy M(2).

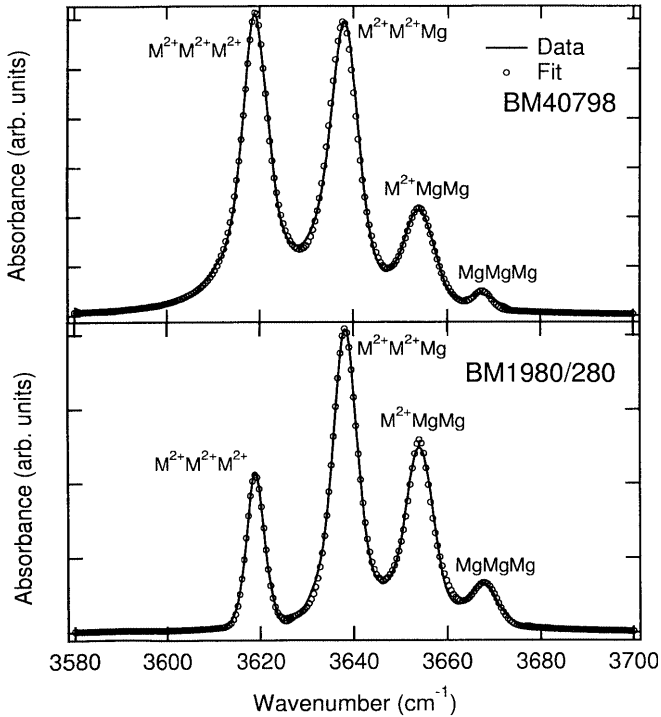


Fig. 6 Two typical infrared absorption spectra from each sample showing fine structure in the hydroxyl-stretching region. *Background* has been removed and *peaks* fitted on the basis of the minimum number required and the lowest residual between observed and fitted spectra

Table 6 Resolved peak areas for the infrared spectra in the hydroxyl-stretching region of both samples. Observed peak areas are those obtained from peak fitting of the spectra and the corresponding M-site occupancies calculated using the model. Site occupancies obtained from neutron diffraction are used to calculate

	Relative peak areas (% total integrated area)				<i>R</i>	Corresponding occupancy		
	MgMgMg	MgMgFe	MgFeFe	FeFeFe		Mg M(1)	Mg M(2)	Mg M(3)
BM40798								
Observed	1.0 (0.4)	12.6 (0.9)	41.0 (1.8)	45.3 (3.2)	0.0073	0.22 (2)	0.22 (2)	0.38 (1)
cm ⁻¹ adjusted ^a	1.6 (0.4)	16 (0.9)	44.2 (1.8)	38.2 (3.2)	0.0066	0.23 (2)	0.16 (2)	0.47 (1)
LRO from neutrons	0.4 (0.1)	7.5 (1.1)	36.2 (1.7)	55.9 (2.8)		0.15 (1)	0.36 (1)	0.23 (2)
Random	1.5	14.1	42.2	42.2		0.25	0.25	0.25
BM1980/280								
Observed	4.2 (0.9)	29.0 (4.4)	46.6 (2.0)	20.2 (3.5)	0.0045	0.31 (4)	0.48 (4)	0.68 (4)
cm ⁻¹ adjusted ^a	5.5 (0.9)	33.3 (4.4)	45.7 (2.0)	15.5 (3.5)	0.0041	0.34 (4)	0.42 (4)	0.75 (4)
LRO from neutrons	10.4 (0.9)	35.2 (1.1)	39.6 (0.9)	14.8 (1.1)		0.48 (1)	0.43 (1)	0.45 (2)
Random	9.4	33.8	40.6	16.3		0.45	0.45	0.45

^a Adjusted linearly using the wavenumber dependency of the molar absorptivity suggested by the data of Skogby and Rossman (1991)

Discussion and conclusions

The anomalous time-dependent behaviour in cell parameters of BM40798, observed as a function of increasing temperature above T_c , in the second of the isothermal data sets is unlikely to be due to sample oxidation in view of the fact that our sample is held in a vanadium can under a high vacuum (vanadium is a highly efficient oxygen getter). The possibility that the sample is still reaching a thermal equilibrium over the time scale of the experiment must be considered.

Site occupancy refinements suggest that in both samples Mn is ordered with a site preference $M(4) \gg M(2) > M(1) > M(3)$. Calculated mean bond lengths of octahedra and mean cation radii in the two samples agree with trends in refined site occupancies and, apart from thermal expansion, increases in the b edge and decreases in the β angle further confirm the partitioning of Mn from M(4).

The site-exchange energy, ΔG , of Mn for exchange between the M(4) site and M(1,2,3) can be calculated from the exchange reaction, which has an equilibrium constant K_D (with $\Delta G = -RT \ln K_D$). This can be defined as

$$K_D = \frac{Mn^{M(4)}[1 - (Mn^{M(1,2,3)})]}{Mn^{M(1,2,3)}[1 - (Mn^{M(4)})]}$$

theoretical peak areas. The peak areas and site occupancies expected from a random mix of $(Mn + Fe) = (M^{2+})$ and Mg are also tabulated. *Figures in parentheses* represent one standard deviation, either in site occupancy or individual peak area

where $Mn^{M(1,2,3)}$ is the average site occupancy of the five smaller sites. The site-exchange energy of Mn for exchange onto the M(4) site in sample BM40798 is $-16.6 \pm 0.5 \text{ kJ.mol}^{-1}$ and in sample BM1980/280 is $-14.9 \pm 0.5 \text{ kJ.mol}^{-1}$. These site-exchange energies are significantly lower than that calculated for an Mn–Mg amphibole with no Fe content (Reece et al. 2000), as one might expect from crystal chemical considerations.

On heating, the partitioning into the octahedral sites starts at 350 °C, with a kinetic relaxation towards a more ordered distribution in the less Mn-rich sample before equilibrium disorder. This kinetic phenomenon has been observed in a very wide range of minerals, from simple oxides to complex silicates such as amphiboles. (Henderson et al. 1996; Redfern et al. 1996, 1997, 1998, 1999a,b, 2000; Harrison et al. 1998, 2000; Reece et al. 2000). Small apparent changes in occupancy within the octahedral strip and not involving the M(4) site below 350 °C may or may not be “real”, but it seems that in sample BM1980/280 Mn first enters the M(2) site from M(1), before the temperature is high enough to enable ordering followed by disordering involving M(4).

Our diffraction data suggest that Fe is strongly partitioned into M(1) and M(3) in sample BM40798, suggesting that this sample cooled much more slowly than BM1980/280, in which a more disordered distribution of ions is observed with Mn displaying the greatest order.

Mössbauer data agree, within error, with Fe site occupancies determined by Rietveld refinement of neutron diffraction data and show that the high-*T* disorder is preserved on cooling.

The use of FTIR spectra in the determination of cation distributions in these amphiboles is limited by a number of factors. Obtaining accurate, reproducible peak areas for the fine structure in the hydroxyl-stretching region is made difficult by errors associated with sample preparation and the presence of a large background that cannot usually be removed with a simple linear baseline. It is likely that a degree of SRO exists in the samples. In the general case of infrared absorption spectra for amphiboles in the OH-stretching region, it is still unclear whether or not the frequency dependence of the transition moment of individual bands in the fine structure has a significant effect on the relative band intensities. This additional uncertainty, allied with the further perturbations to the OH fine structure that may arise from the effects of clustering or avoidance, which changes SRO compared with LRO, makes the quantitative interpretation of such data problematic.

Acknowledgements This work was supported by NERC via grant no. GR3/11741. We are grateful for the anonymous reviewers' comments.

References

- Burns RG, Strens RGJ (1966) Infrared study of the hydroxyl bands in clinoamphiboles. *Science* 153: 890–892
- Della Ventura G, Robert JL, Hawthorne FC (1996) Infrared spectroscopy of synthetic (Ni, Mg, Co)-potassium-richite. In: Dyar MD, McCammon C, Schaefer MW (eds) *Mineral spectroscopy: a tribute to Roger G. Burns*. The Geochemical Society, pp 55–63, Washington DC, USA
- Droop GTR (1987) A general equation for estimating Fe^{3+} concentrations in ferromagnesian silicates and oxides from microprobe analyses, using stoichiometric criteria. *Mineral Mag* 51: 431–435
- Evans BW, Ghiorso MS (1995) Thermodynamics and petrology of cumingtonite. *Am Mineral* 80: 649–663
- Ghose S, Weidner JR (1972) Mg^{2+} – Fe^{2+} order–disorder in cumingtonite, $(Mg,Fe)_7Si_8O_{22}(OH)_2$: a new geothermometer. *Earth Planet Sci Lett* 16: 346–354
- Harrison RJ, Redfern SAT, O'Neill HStC (1998) The temperature dependence of the cation distribution in synthetic hercynite ($FeAl_2O_4$) from in-situ neutron structure refinements. *Am Mineral* 83: 1092–1099
- Harrison RJ, Redfern SAT, Smith RI (2000) In-situ study of the $R\bar{3}$ to $R\bar{3}c$ phase transition in the ilmenite–hematite solid solution using time-of-flight neutron powder diffraction. *Am Mineral* 85: 194–205
- Hawthorne FC (1983) The crystal chemistry of the amphiboles. *Can Mineral* 21: 173–480
- Hawthorne FC, Della Ventura G, Robert J-L (1996) Short-range order and long-range order in amphiboles: a model for the interpretation of infrared spectra in the principal OH-stretching region. In: Dyar MD, McCammon C, Schaefer MW, (eds) *Mineral spectroscopy: a tribute to Roger G. Burns*. The Geochemical Society. pp 49–54
- Henderson CMB, Knight KS, Redfern SAT, Wood BJ (1996) Temperature dependence of octahedral cation site exchange in olivine determined by in situ, time-of-flight, neutron powder diffraction. *Science* 271: 1713–1715
- Hull S, Smith RI, David WIF, Hannon AC, Mayers J, Cywinski R (1992) The POLARIS powder diffractometer at ISIS. *Physica (B)* 180: 1000–1002
- Larson AC, Von Dreele RB (1994) GSAS general structure analysis system. LAUR 86–748, Los Alamos National Laboratory, Los Alamos, NM 87545, USA
- Law AD (1976) A model for the investigation of hydroxyl spectra of amphiboles. In: Strens RGJ (ed) *The physics and chemistry of rocks and minerals*. Wiley, London, pp 677–686
- Leake BE, Wooley AR, Arps CES, Birch WD, Gilbert MC, Grice JD, Hawthorne, FC, Kato A, Kisch HJ, Krivovichev VG, Linthout K, Laird J, Mandarino JA, Maresch WV, Nickel EH, Rock NMS, Schumacher JC, Smith DC, Stephenson NCN, Ungaretti L, Whittaker EJW, Youzhi G (1997) Nomenclature of the amphiboles: Report of the Subcommittee on Amphiboles of the International Mineralogical Association, Commission on New Minerals and New Mineral Names. *Mineral Mag* 61: 295–321
- Myers ER, Heine V, Dove MT (1998) Thermodynamics of Al/Al avoidance in the ordering of Al/Si tetrahedral framework structures. *Phys Chem Miner* 25: (6), 457–464
- Redfern SAT, Henderson CMB, Wood BJ, Harrison RJ, Knight KS (1996) Determination of olivine cooling rates from metal cation ordering. *Nature* 381: 407–409
- Redfern SAT, Henderson CMB, Knight KS, Wood BJ (1997) High-temperature order-disorder in $(Fe_{0.5}Mn_{0.5})_2SiO_4$ and $(Mg_{0.5}Mn_{0.5})_2SiO_4$ olivines: an in situ neutron diffraction study. *Eur J Mineral* 9: 287–300
- Redfern SAT, Knight KS, Henderson CMB, Wood BJ (1998) Fe–Mn cation ordering in fayalite–tephroite $(Fe_xMn_{1-x})_2SiO_4$ olivines: a neutron diffraction study. *Mineral Mag* 62: 607–615
- Redfern SAT, Harrison RJ, O'Neill HStC, Wood DRR (1999a) Thermodynamics and kinetics of cation ordering in $MgAl_2O_4$ spinel up to 1600 °C from in-situ neutron diffraction. *Am Mineral* 84: 299–310
- Redfern SAT, Welch MD, Henderson CMB, Knight KS (1999b) In situ high-*T* neutron diffraction studies of non-convergent order/

- disorder in minerals: from simple oxides to complex silicates. *Phase Transitions* 69: 17–34
- Redfern SAT, Artioli G, Rinaldi R, Henderson CMB, Knight KS, Wood BJ (2000) Octahedral cation ordering in olivine at high temperature. II: an in situ neutron powder diffraction study on synthetic MgFeSiO_4 (Fa50). *Phys Chem Miner* 27: 630–637
- Reece JJ, Redfern SAT, Welch MD, Henderson CMB (2000) Mn–Mg disordering in cummingtonite: a high-temperature neutron powder diffraction study. *Mineral Mag* 64: 255–266
- Rietveld HM (1969) A profile refinement method for nuclear and magnetic structures. *J Appl Crystallogr* 2: 65–71
- Shannon RD (1976) Revised effective ionic radii and systematic studies of interatomic distances in halides and chalcogenides. *Acta Crystallogr*, A32: 751–767
- Skogby H, Rossman GR (1991) The intensity of amphibole OH bands in the infrared absorption spectrum. *Phys Chem Miner* 18: 64–68
- Strens RGJ (1974) The common chain, ribbon and ring silicates. In: Farmer VC (ed) *The infrared spectra of minerals*. Mineralogical Society of America, Washington DC, pp 305–330
- Whittaker EJW (1979) Clustering of cations in amphiboles. *Phys Chem Miner* 4: 1–10